Controlling the Physical and Biological Properties of Highly Fluorescent Aqueous Quantum Dots Using Block Copolymers of Different Size and Shape

Johannes Ostermann,[†] Jan-Philip Merkl,[†] Sandra Flessau, Christopher Wolter, Andreas Kornowksi, Christian Schmidtke, Andrea Pietsch, Hauke Kloust, Artur Feld, and Horst Weller*

Institute of Physical Chemistry, University of Hamburg, Grindelallee 117, 20146 Hamburg, Germany. [†]These authors contributed equally to this work.

ABSTRACT The phase transfer of fluorescent CdSe based quantum dots (QDs) while retaining their properties and offering some advantages concerning the stability and functionalization characteristics is an important and intensively investigated field of research. Here we report how to tune and control the properties of CdSe/CdS/ZnS core—shell—shell QDs in water, using poly(isoprene-*block*-ethylene oxide) (PI-*b*-PEO) as a versatile system of amphiphilic diblock copolymers for the micellular encapsulation of nanoparticles (NPs). We show the synthesis of a novel PI-*b*-$(PEO)_2$ miktoarm star polymer and how this different architecture besides the variation of the polymers' molecular weight gives us the opportunity to control the size of the built constructs in water between 24 and 53 nm. Because of this size control, an upper limit of the construct's diameter for the cellular uptake could be determined by a systemic study with human alveolar epithelial cells (A549) and murine macrophage leukemia cell (RAW-264.7). Furthermore, fluorescence quenching experiments with copper(II) and iron(III) ions show a strong influence of the used polymer on the shielding against these ions. This enables us to control the permeability of the polymer shell from very porous shells, which allow an almost complete cation exchange up to very dense shells. These even offer the possibility to perform copper(I) catalyzed click reactions while keeping the fluorescence of the QDs. All these results underline the huge variability and controllability of the PI-*b*-PEO diblock copolymer system for the encapsulation and functionalization of nanoparticles for biological applications. As a general trend, it can be stated that those coatings, which were most stable against quenchers, also showed the best resistivity with respect to unspecific cellular uptake.

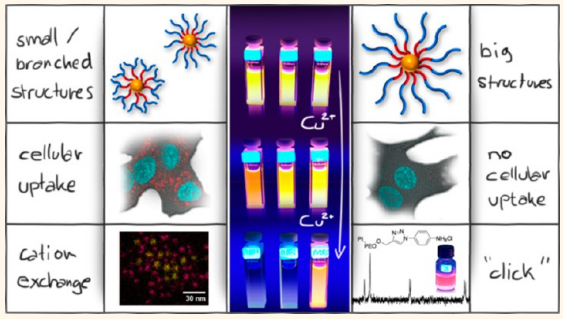

KEYWORDS: quantum dots · phase transfer · amphiphilic diblock copolymer · micelles · fluorescence quenching · cellular uptake · copper mediated click reaction

The use of highly fluorescent quantum dots (QDs) as labels for biological imaging is a very promising approach. QDs possess extraordinary optical properties, such as high extinction coefficients, broad absorption, narrow, adjustable emission and high photostabilities.[1−3] However, to obtain QDs with a narrow size distribution and high photoluminescence quantum yields, a synthesis in organic media is essential.[2,4] Thus, for biological applications, a phase transfer is required while retaining the optical properties of the nanoparticles. Several strategies for this phase transfer have been developed, such as ligand exchanges with polyethylene oxide (PEO) derivatives,[5,6] encapsulation in amphiphilic di- or triblock copolymers,[7,8] silica shells[9] or polymer beads.[10]

Typically, in biological *in vitro* and *in vivo* studies, the concentration of the biolabel is very low and salt concentrations are very high. These conditions already highlight the requirements on water-soluble QDs, and the ligand system. The particles must be stable at very high dilutions without any aggregation or loss of their properties. The ligand system must provide an excellent shielding against the biological media, which includes proteins, small organic molecules and the high amount of present ions. Especially the latter can have a strong impact on fluorescence properties and possibly even on the stability of the ligand shell.

* Address correspondence to weller@chemie.uni-hamburg.de.

Received for review July 22, 2013 and accepted September 13, 2013.

Published online September 13, 2013
10.1021/nn4037859

Finally, the ligand system has to offer a functionalization site, at which typical bioconjugation reactions can be carried out to build a specific label. For a better accessibility, this functionalization site should be presented at the outer shell.

A very potent and frequently used coupling method for biologically relevant molecules is the copper(I)-catalyzed azide alkyne Huisgen cycloaddition. These reactions can be performed under very mild conditions; the tolerance to functional groups is huge and the built products do not undergo hydrolysis reactions.[11] Thus, copper(I) mediated 'click' chemistry can be utilized easily for the functionalization and coupling of biomolecules to nanoparticles once the phase transfer has been performed. Such coupling reactions on nanoparticles have already been demonstrated for several systems.[12,13] Unfortunately, the adoption of this coupling strategy to QDs has shown to result in strong fluorescence quenching during the reactions.[14] This can be explained by the permeable nature of the used ligand systems for copper ions. Once a copper ion diffuses in direct contact to the QD surface, the bandgap emission fluorescence is quenched statically and irreversibly, leading to drastic loss of fluorescence quantum yields due to cation exchange or formation of Cu(I) species.[15,16] In contrast to this surface adsorption, copper cluster-seeded quantum dots, namely, cadmium selenide[17] and zink sulfide,[18,19] exhibit emission from dopant states while bandgap luminescence is quenched. This quenching of the bandgap and the appearance of dopant emission are temperature dependent and were correlated with different chemical doping reactions such as surface adsorption and lattice incorporation.[18]

Quenching of the luminescence during copper catalyzed cycloaddition reactions can be avoided by using strained cyclooctyne derivatives. However, cyclooctyne derivatives are expensive and need to be coupled to the target molecule, resulting in a bigger synthetic effort.[20−22] Therefore, a strategy or ligand system, allowing classic copper(I)-catalyzed click chemistry, would overcome a lot of problems in coupling biological relevant molecules to QDs for the use as biolabels. Here we present, to the best of our knowledge, the first click reaction in the presence of QD by using a micellular encapsulation technique which provides a significantly improved shielding against quenching ions while retaining the fluorescence properties of the QDs. Permeability control of the organic layer is important for the *in vivo* use of the particles with respect to possible ion leaching due to cation exchange reaction. The fluorescence of semiconductor nanocrystals is very sensitive to its surface states and can thus be influenced by adsorbed molecules,[23] epitaxially grown nanoparticles[24] and ions.[20] Thus, fluorescence quenching experiments are commonly used to study the environment surrounding a QD.[25−27]

TABLE 1. Analytical Data Concerning Molecular Weight and Aggregation Properties of Used Diblock Copolymers

name	M_w[a] (g/mol)	M_n[a] (g/mol)	M_w/M_n[a]	M% PEO[b]	cac[c] (μM)	d_H[d] (nm)
PI-*b*-PEO 1	4600	4300	1.06	68	0.60	16.8
PI-*b*-PEO 2	8100	6600	1.22	73	0.35	21.9
PI-*b*-PEO 3	9900	9000	1.09	65	0.27	24.8
PI-*b*-PEO 4	11900	10500	1.13	67	0.20	27.4
PI-*b*-PEO 5	14300	13400	1.07	70	0.15	28.0
PI-*b*-$(PEO)_2$ Y	8400	7300	1.15	73	0.36	15.9

[a] SEC analysis using PEO standards. [b] NMR analysis. [c] Fluorescence studies using pyrene as fluorophore.[42] [d] DLS measurements, mean diameter by volume.

We recently demonstrated a versatile encapsulation system for nanoparticles, based on an amphiphilic poly(isoprene-*block*-ethylene oxide) (PI-*b*-PEO) diblock copolymer. The particles, encapsulated in micelles, keep their unique optical properties, while the PI-*b*-PEO diblock copolymer offers some advantages. The terminal double-bonds of the polyisoprene (PI) chain offer the possibility of cross-linking the hydrophobic core of the micelle. Poly(ethylene oxide) (PEO) is a water-soluble polymer, which is known to be nontoxic, used to reduce unspecific protein absorption and, therefore, provides a good biocompatibility. Finally, it offers the possibility of functionalization at the terminal alcohol function prior or subsequent to the encapsulation of nanoparticles.[28,29]

Herein, we report the influence of the PI-*b*-PEO's size and architecture on the encapsulation of QDs and on the properties of the obtained structures. Therefore, several differently sized PI-*b*-PEOs and one new miktoarm star, consisting of two PEO and one PI chain (PI-*b*-$(PEO)_2$), have been synthesized. The differences between the branched and the linear polymers concerning their aggregation behavior in water have been examined. All polymers have been used for the phase transfer of QDs to investigate size and architecture effects of the polymers on the QDs. This includes the determination of the constructs' physical properties like size and stability against quenching by copper ions and the determination of their biological properties, namely, the interaction with two different cell lines.

RESULTS AND DISCUSSION

Synthesis and Characterization of the PI-*b*-PEO Block Copolymers and Aggregation Behavior. For the investigation of the influence of polymer lengths on the properties of encapsulated nanoparticles, we synthesized five different PI-*b*-PEO block copolymers with a M_n between 4300 and 13 400 g/mol according to the known procedure using standard anionic polymerization techniques.[28,30,31] The obtained polymers show low polydispersities (see Table 1), and since the polymerization reactions of isoprene were carried out in THF, they exhibit a high content of 1,2- and 3,4-linked units in the hydrophobic region.[32] This microstructure offers the

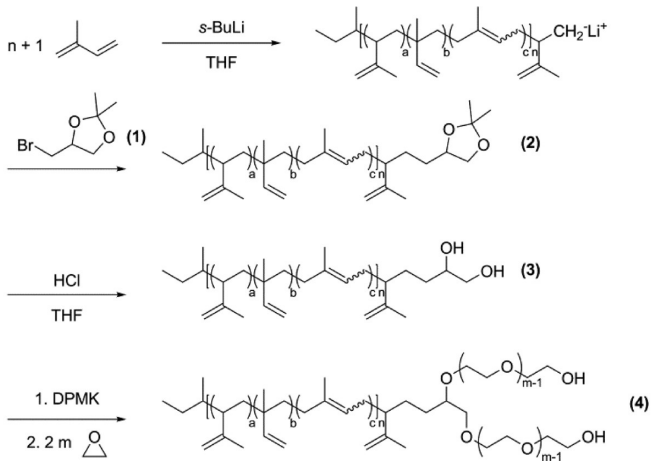

Scheme 1. Synthetic route for the amphiphilic PI-*b*-$(PEO)_2$ miktoarm star.

opportunity for cross-linking polyisoprene chains with each other by radical initiators.[33] All polymers bear an alcohol function at the hydrophilic PEO end which makes them accessible for functionalization[29,34] and/or coupling of biomolecules. The PI chain end is blunt and, therefore, not accessible for functionalization or specific interactions.

During the last years, several star-shaped polymers and miktoarm stars have been synthesized[35−38] and investigated concerning their aggregation properties. Since the architecture has a strong influence on some important parameters like the critical micelle concentration,[39] aggregation number,[36] and the hydrodynamic diameter[36,40] of the aggregated structures, we synthesized one amphiphilic miktoarm star consisting of one PI and two PEO chains to investigate the influence of the architecture on the encapsulation of nanoparticles. Therefore, the anionic polymerization of isoprene was terminated using 4-(bromomethyl)-2,2-dimethyl-1,3-dioxolane (**1**) which can easily be obtained in a two-step synthesis starting from epibromohydrine. This leads to an acetal end group, which can be deprotected using HCl in THF to yield two alcohol functions as new starting points for the subsequent polymerization of ethylene oxide (see Scheme 1). All polymers show a very similar ratio of hydrophilic to hydrophobic blocks which was determined by SEC and ^{1}H NMR analysis.

The aggregation behavior of the five synthesized polymers in water was investigated by building micellular constructs using a similar method as for the encapsulation of nanoparticles. The samples were dissolved in THF and injected into water, followed by heating to 80 °C for four hours to remove most of the THF. Dynamic light scattering measurements show the expected behavior between the molecular weight of the PI-*b*-PEO and the determined hydrodynamic radius of the micellular aggregates. As has already been published for other A_2B miktoarm stars,[36,40] we observed a significantly smaller hydrodynamic radius of the PI-*b*-$(PEO)_2$ miktoarm star micelle than that for for the comparable linear PI-*b*-PEO micelle (see Figure 1a).

Investigation of the critical aggregation concentration (cac) of the different polymers again shows a systemic correlation to the polymer size, as can be seen in Table 1. Although all cac's are in the same dimension, the value shows a significant decrease with increasing polymer size. This finding is consistent with literature reports on the correlation between the chain length of the insoluble block and the cmc value.[41] For the miktoarm star, we determined a slightly higher cac than that for the comparable diblock copolymer (PI-*b*-PEO 2), which has been explained for PS-*b*-$(PEO)_2$ miktoarm stars by Gibanel *et al.* by the higher steric hindrance of the branched polymer during the micellation process.[39]

Encapsulation of QD Using Micellular Encapsulation Technique. The encapsulation of CdSe/CdS/ZnS core−shell−shell nanoparticles was carried out with the described block copolymers following a standard procedure for this system.[28] The nanoparticles' native ligands were replaced by a short polyisoprene (M_n = 1400 g/mol) bearing a diethylenetriamine function (DETA) which has already shown good properties as an anchor group for this particle system. After the QDs were mixed with a 300-fold excess of block copolymer in THF, 2,2′-azobis-(2-methylpropionitrile) (AIBN) (1/3 relating to the number of double bonds in the PI-*b*-PEO) was added and the mixture was injected into water, using a flow controlled mixing device. Finally, the mixture was heated to 80 °C to enable the cross-linking process and to evaporate the THF, followed by a sucrose gradient ultracentrifugation to remove excess empty micelles.

Despite the complexity of the system, DLS studies of the built constructs also show the expected relation to the size of the used block copolymer and hydrodynamic diameters between 24 and 53 nm can be adjusted (see Figure 1a). This stringent behavior and its high reproducibility turns the used block copolymers into a very powerful tool for the phase transfer of nanoparticles

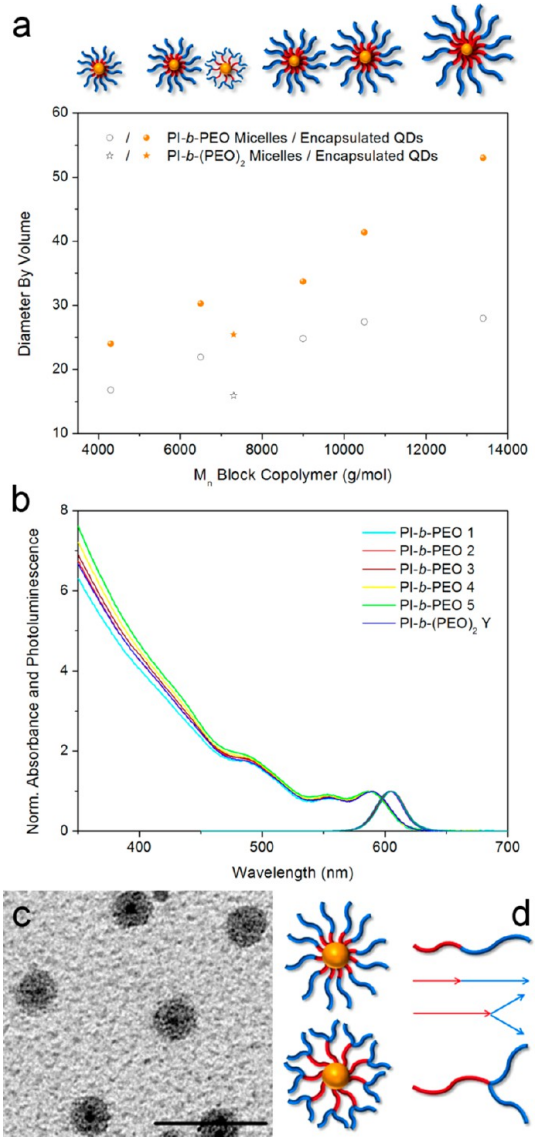

Figure 1. (a) Hydrodynamic diameters for empty micelles and encapsulated particles, determined by dynamic light scattering (DLS, volume mean) *vs* the molecular weight of the used PI-*b*-PEO; black hollow circles, star PI-*b*-PEO micelles; orange filled circles, star QDs encapsulated in PI-*b*-PEO. (b) Absorption and emission spectra of PI-*b*-PEO encapsulated QDs in water. (c) TEM images of PI-*b*-PEO 5 encapsulated QDs. Scale bars represent 50 nm; contrast was achieved by OsO_4 staining. (d) Schematic illustration of the expected differences between the linear and miktoarm block copolymer.

while keeping their properties and having control over the size of the resulting constructs. Again we achieve much smaller hydrodynamic diameters for the nanoparticles encapsulated in the miktoarm star compared to those for the linear diblock copolymers, which makes further investigation concerning the shielding and biological compatibility of these constructs very interesting.

As we expected, the absorption and emission properties of all the prepared samples are not influenced by the different block copolymers (see Figure 1b). Fluorescence quantum yields of the constructs are almost the same, showing no significant relation to the polymer size or architecture. TEM images (see Figure 1c; Figure SI 1) show predominately single encapsulated QDs. The samples were stained with OsO_4 to enhance the contrast of the polymer. Since OsO_4 is known to stain double-bonds selectively,[43] the dark corona around the particles is assumed to be mainly polyisoprene.

Cellular Uptake. Since the influence of the polymers' size and architecture on the size of the encapsulated quantum dots was very strong, the investigation of the QDs' behavior in biological systems was another aim. Therefore, experiments with human alveolar epithelial cells (A549) were carried out to investigate toxicity and the unspecific cellular uptake. As has been recently reported by us and other groups, the unspecific uptake of aqueous nanocrystals is strongly dependent on the chosen experiment conditions. Serum containing medium, for example, reduces the unspecific cellular uptake of nanocrystals, which seems to be a result of the protein corona formed around the nanocrystals.[29,44,45] Experiments with our constructs under biologically relevant conditions in fact show no unspecific uptake at all (see Supporting Information for conditions and confocal microscope images, Figure SI 3). This provides the opportunity to use this system as a tool for specific targeting of certain cells *via* bound recognition molecules in the future, since no unspecific background has to be expected.

Further investigations aimed to enforce the uptake of our constructs by changing the experiment conditions. Therefore, we worked under very radical conditions in serum free media, with very high nanocrystal concentrations and long incubation times. As can be seen from the confocal microscope images (Figure 2), we observed cellular uptake for all tested constructs in A549 cells except for the quantum dots encapsulated in the biggest diblock-copolymer (PI-*b*-PEO 5). Even under these extreme conditions after 20 h of incubation, the unspecific uptake is somehow hindered, which coincides with the information on cellular uptake we earlier gained for encapsulated quantum dots in a similar sized diblock copolymer.[28] These findings lead us to the assumption that the hydrodynamic diameter and therefore also the polymer size determines whether the unspecific uptake takes place. To see if this trend is also valid for other cell lines, some of the constructs (PI-*b*-PEO 1, PI-*b*-PEO 2, PI-*b*-PEO 5, and PI-*b*-$(PEO)_2$ Y) were tested on murine macrophage leukemia cells (RAW-264.7) (Figure 2e–g). As we expected, the uptake of encapsulated QDs in macrophages is huge for the smaller constructs (PI-*b*-PEO 1, PI-*b*-PEO 2, and PI-*b*-$(PEO)_2$Y) and almost not observable for the biggest polymer (PI-*b*-PEO 5), emphasizing the previously observed size dependent effect. Since the investigated cells show no obvious degeneracy

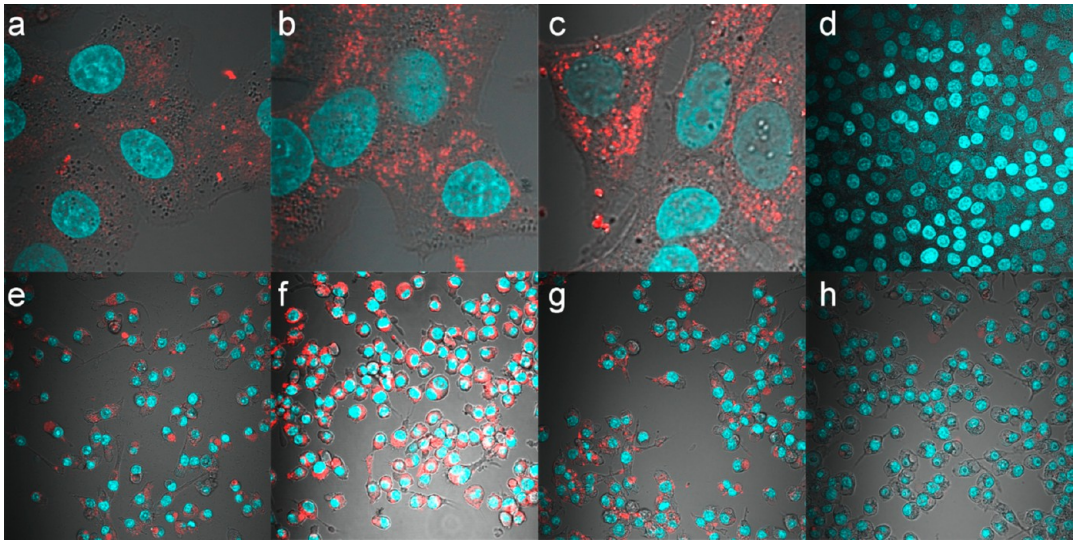

Figure 2. Confocal microscope images of (top row) A549 cells incubated with 1 μM of PI-*b*-PEO encapsulated quantum dots after an incubation time of 20 h: (a) PI-*b*-PEO 1; (b) PI-*b*-PEO 2; (c) PI-*b*-$(PEO)_2$ Y; (d) PI-*b*-PEO 5. (Bottom row) RAW-264.7 cells incubated with 1 μM of PI-*b*-PEO encapsulated quantum dots after 20 h of incubation: (e) PI-*b*-PEO 1; (f) PI-*b*-PEO 2; (g) PI-*b*-$(PEO)_2$ Y; (h) PI-*b*-PEO 5. Red areas arise from QD fluorescence. The cells nuclei were counterstained with Hoechst 33342 (blue).

even after such a long time of incubation with quantum dots, no further toxicity tests were executed. This is supported by recent investigations of similarly prepared samples, which showed no toxicity in standard WST8 and LDH tests.[28,29] The findings concerning the toxicity suggest a dense shell around the particles, which prevents leaching of cadmium ions. Interestingly, the fluorescence intensity for the smallest construct (PI-*b*-PEO 1) in the cell experiment seemed to be lower compared to that for the other constructs (Figure 2a), which could be an indication for a quenching process, due to the smaller protecting polymer shell. To gain more knowledge about the permeability of the polymer shell around the nanoparticles, fluorescence quenching experiments were conducted.

Fluorescence Quenching Experiments. The fluorescence quantum yield of quantum dots is very sensitive to the presence of electron acceptors and chemical changes at the nanocrystal surface. Thus, fluorescence quenching experiments conveniently indicate whether and to what extent molecules or ions can penetrate the surrounding ligand shell. This information is also of strong biological relevance, because serum compounds, as well as receptors or target molecules, may come into direct contact with the nanocrystal surface or ionic compounds of the nanocrystals may leak out into the biological environment. Thus, the biological response to nanoparticles will obviously depend on the shielding of the nanocrystals by the ligand shell.

In photochemistry, two different mechanisms of fluorescence quenching are distinguished. So-called dynamic quenching occurs upon collisions of the excited dye with a quencher and is usually dominated by diffusion processes. Static quenching, on the other hand, occurs when the quencher forms a nonfluorescent ground state complex with the dye. In case of quantum dots, the latter corresponds to surface adhesion of the quencher or even a chemical reaction like ion exchange. In both cases, the integral fluorescence intensity is decreased as can be seen in the fluorescence spectra. In fluorescence lifetime measurements, distinct differences show up in the decay curves, eq 1.

$$I(t) = Ae^{-t/\tau(Q)} \quad (1)$$

Dynamic quenching opens an additional decay channel of the excited state. As a consequence, the decay time, $\tau(Q)$, is shortened, but the signal height at $t = 0$ (number of counts), A, stays constant. In contrast, $\tau(Q)$ remains constant and A decreases as a result of static quenching, because one fraction of particles is completely quenched, whereas the other remains unaffected.

Fluorescence quenching is usually described by the Stern–Volmer-formalism, eq 2. F_0 is the fluorescence intensity in absence of a quencher, $F(Q)$ is the fluorescence intensity depending on the quencher concentration, K_{SV} is the Stern–Volmer-constant, and $[Q]$ is the quencher concentration.[46]

$$\frac{F_0}{F(Q)} = 1 + K_{SV}[Q] \quad (2)$$

For static quenching, K_{SV} corresponds to the equilibrium constant of complex formation, whereas it equals the product of the bimolecular quenching rate constant, k_q, and the fluorescence decay time in the absence of quencher, τ_0. F_0 and $F(Q)$ can be determined in both cases from the integral of the fluorescence spectra or, if the spectral distribution remains constant upon quenching, from the integral of the

decay curves at a given wavelength. For dynamic quenching, the ratio of F_0 and $F(Q)$ can also be expressed by the ratio of τ_0 and $\tau(Q)$. Equation 2 can then be written as

$$\frac{F_0}{F(Q)} = \frac{\tau_0}{\tau(Q)} = 1 + k_q \tau_0 [Q] \quad (3)$$

To study the permeability of the various polymer shells, we performed quenching experiments with copper(II) acetate for six samples, encapsulated with linear PI-*b*-PEO (PI-*b*-PEO 1−5) and star shaped PI-*b*-$(PEO)_2$ Y polymers. Aliquots of copper(II) acetate stock solution were added to a QD solution, and emission and absorption spectra, as well as the fluorescence decay curves, were measured. The results from the quenching analysis are summarized in Figure 3. As an overview, the normalized fluorescence intensities obtained from the integral fluorescence spectra, $F(Q)/F_0$, are plotted against the equivalents of copper added to the QD solution (Figure 3a). Copper is known to quench the fluorescence of QDs irreversibly and statically due to the formation of copper sulfide/selenide.[20] This observation was confirmed with the native QD sample in organic solution (black bars in Figure 3a). We observed total quenching within seconds after adding 5 equiv of copper per particle (equiv pp). After phase transfer, the protection of the particles against quenching copper ions is strongly enhanced and depends on the size of the used polymer. Compared to reported results with PEO-amine[20,47] of similar molecular weight but without hydrophobic blocks and L-cystein[48] based ligand systems, we observed a significantly higher shielding. This indicates that it is mainly the thickness of the hydrophobic part of the ligand shell (red region in Figure 1) which hinders solution compounds to reach the nanocrystal surface. Accordingly, we found as a general trend that within the series of linear polymers the bigger ones with higher molecular weight (PI-*b*-PEO 3−5) achieve better shielding than the smaller ones. It should be pointed out that the highest amount of quencher addition would correspond to 40% ion exchange of Zn^{2+} and Cd^{2+} against Cu^{2+}, if the surface would be freely accessible. The very moderate quenching effect indicates how effective shielding in all samples is. A more careful analysis shows that the quenching is mainly associated with a drop of the initial height of the decay curves (Figure 3b) and to a smaller extent with a decrease in decay time (Figure 3c), meaning static quenching dominates over dynamic. Only at copper additions exceeding 200 equiv per particles a slight decrease of the excited state lifetime is observed (a factor of 2 at maximum for PI-*b*-PEO-1). We also notice that the first addition of Cu^{2+} (corresponding to ~35 euiv pp) leads to the relative strongest static quenching effect in all cases. We assume that this finding is due to a small fraction of particles, in which the shielding is less optimal,

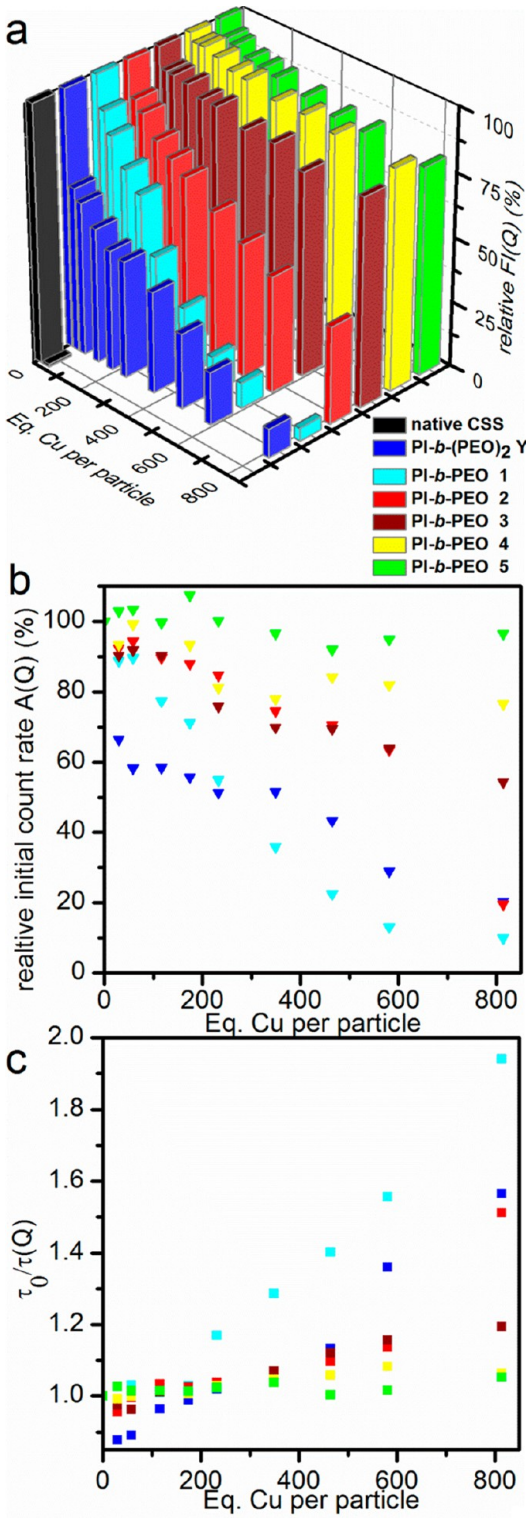

Figure 3. (a) Relative fluorescence intensities of QDs encapsulated with PI-*b*-PEO 1 (cyan), PI-*b*-PEO 2 (red), PI-*b*-PEO 3 (brown), PI-*b*-PEO 4 (magenta), PI-*b*-PEO 5 (green), and miktoarm star shaped PI-*b*-$(PEO)_2$ Y (dark blue) after the addition of aliquots Cu^{2+}. The data were taken from the fluorescence spectra. Native QD in organic solution are shown as a black bar (10× enlarged intensity). (b) Initial counts (signal height) of the fluorescence decay curves, (same color code as in (a)). (c) Stern−Volmer plot of the fluorescence lifetimes (τ_0/τ) indicating dynamic quenching (same color code as in (a)).

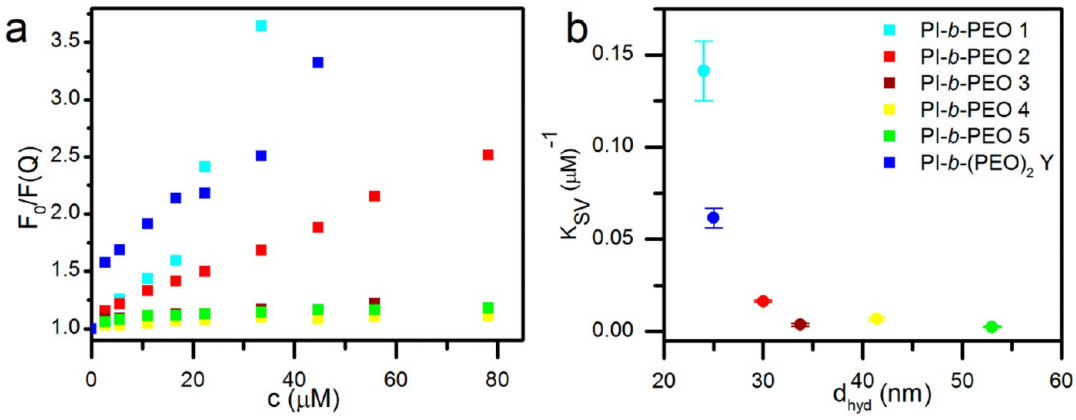

Figure 4. (a) Stern–Volmer plot of encapsulated QD (*c*(QD) = 0.1 μM) with PI-*b*-PEO 1 (cyan), PI-*b*-PEO 2 (red), PI-*b*-PEO 3 (brown), PI-*b*-PEO 4 (yellow), PI-*b*-PEO 5 (green), and miktoarm star shaped PI-*b*-(PEO)$_2$ Y (dark blue) by quenching with Cu(ac)$_2$ (squares). (b) Stern–Volmer constant plotted against the hydrodynamic diameter (circles).

probably due to nonperfect self-assembly during phase transfer.

Some special features were observed for the star shape miktoarm PI-*b*-PEO Y encapsulated QDs. First, static quenching at low quencher concentrations is more pronounced than for the linear components of comparable molecular weight (PI-*b*-PEO 2) (initial drop of the intensity bars in Figure 3a). Because of the geometry of this polymer, we expect a lower number of ligands being bound per particles compared to the linear polymers.[36] This would result in a less dense or thinner PI moiety of ligand shell allowing Cu^{2+} an easier access to the QD surface. Curiously, the initial quenching at low Cu^{2+} concentrations results in a slight increase of the fluorescence decay time (blue squares in Figure 3c). This concave curvature of the $\tau_0/\tau(Q)$ plot of PI-*b*-PEO Y was confirmed in numerous experiments. The reason for this behavior is seen in the fact that the $\tau(Q)$ values reflect an average decay time of the nanocrystal ensemble concerning the stretched exponential fit routine. Assuming the fraction of less perfectly encapsulated QDs having a lower fluorescence quantum yield and therefore a shorter fluorescence decay time, this fraction is missing in the decay curve after the first quencher addition. As a result, the average decay time of the remaining fluorescent fraction increases. We observed the same behavior according shielding, dynamic quenching and concave curvature of the τ_0/τ plot in quenching experiments with Fe^{3+} as a quencher. The results are shown in the Supporting Information (Figure SI 5) together with further details on the dynamic quenching process (Figure SI 6).

The Stern–Volmer plots of the integral fluorescence intensity obtained from the fluorescence spectra are shown in Figure 4a. Astonishingly, all curves except the one of PI-*b*-PEO 1 show an almost perfect linear slope, although rather different fluorescence quenching processes were clearly observed in the time-resolved measurements. This finding underlines the importance of combined static and dynamic fluorescence investigations for obtaining detailed information on the ligand shell of fluorescent nanocrystals. At a quencher concentration of 15 μM, the Stern–Volmer plot of the sample with the low molecular weight polymer shell, PI-*b*-PEO 1, changes its slope, indicating a more effective quenching at higher concentrations. This is understood by the less effective shielding and the thereof resulting formation of larger CuS moieties at the surface of the nanocrystals and supported by absorption spectra (Figures 5 and SI8. In Figure 4b, the Stern–Volmer constant K_{SV} is plotted against the hydrodynamic diameter. It can be seen that in the range between d_{hyd} = 20 and 35 nm the shielding depends strongly on the size of the obtained construct. An optimum hydrodynamic diameter of about 35 nm is required for a good protection of the nanocrystals (PI-*b*-PEO 3).

We also recorded absorption spectra during the fluorescence quenching experiments. As expected, changes at very low quencher additions are hard to determine (see Supporting Information). At higher quencher concentrations, spectral changes are clearly visible, which are in accordance with copper sulfide formation and the more detailed results from the fluorescence quenching experiments. The corresponding data are shown in the Supporting Information (Figures SI 7–9)

Reaction between Copper Ions and QDs. For practical applications as "clickable" biolables, long-term stability against copper ions is important. We therefore added 2000 equiv of Cu^{2+} per particle to the QD samples corresponding total ion exchange within the nanocrystal core and shell, and recorded the absorption spectra after 4 days of incubation (Figure 5a). In all cases except the PI-*b*-PEO 5 samples, a strong signal in the near-infrared region was detected due to copper sulfide/selenide formation. Kriegel *et al.* explained these bands by localized surface plasmons of nonstoichiometric ($x > 0$) copper chalkogenide nanoparticles such as

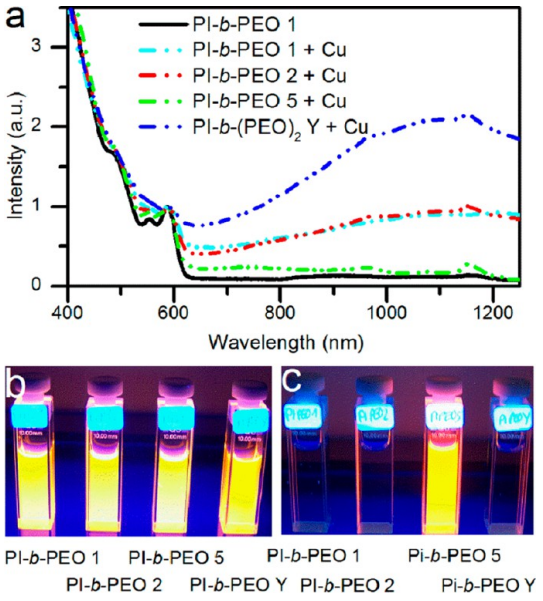

Figure 5. (a) Absorption spectra of the QD constructs after 4 days (dashed lines) incubation with 2000 equiv of Cu(II) per QD. The spectra were normalized to the first absorption maximum. A blank sample with $Cu(II)ac_2$ solution did not show any comparable absorption, and the spectrum of PI-*b*-PEO 1 encapsulated QD is shown as a black solid line. (b and c) Photographs of aqueous QDs with and without addition of Cu^{2+}. Related emission spectra are shown in Figure SI 10.

$Cu_{2-x}S$ and $Cu_{2-x}Se$.[49] Highest reactivity of Cu^{2+} was observed for the miktoarm star shaped polymer (PI-*b*-$(PEO)_2$ Y) particles, where the QD absorption almost completely vanished. Much to our delight, we found that sample PI-*b*-PEO 5 exhibits only very minor changes in the absorption spectra and that the fluorescence is almost completely retained even after these crude four days incubation conditions (Figure 5b,c).

To further investigate the copper sulfide/selenide formation, TEM element mappings were performed of the above-mentioned samples after 1 month of incubation. The samples were purified to remove excess copper ions by washing three times with water in a membrane filter. No copper was found in the third washing solution by atomic absorption spectroscopy (AAS). As expected, the mappings for the long-term incubated samples exhibit clear differences between the investigated samples (see Figure 6). Part a of the figure shows a gallery of a HADF STEM, Cd-L, Se−L, and Cu−K EDX mappings for the PI-*b*-$(PEO)_2$ Y sample, and part b shows the respective images for PI-*b*-PEO 5 encapsulated QDs. As seen in the HAADF image of Figure 6b, the sample consists of a fraction of larger and a fraction of smaller particles and is rather polydisperse in total. Some particles can only be found in the Cd map, others in the Cu map, whereas Se is found in all particles. Also the superposition of the Cd and Cu maps (part c) yields the same morphology pattern as the HAADF image. Thus, a fraction of particles is almost completely converted into copper selenide, whereas others still mainly consist of the original QD composition.

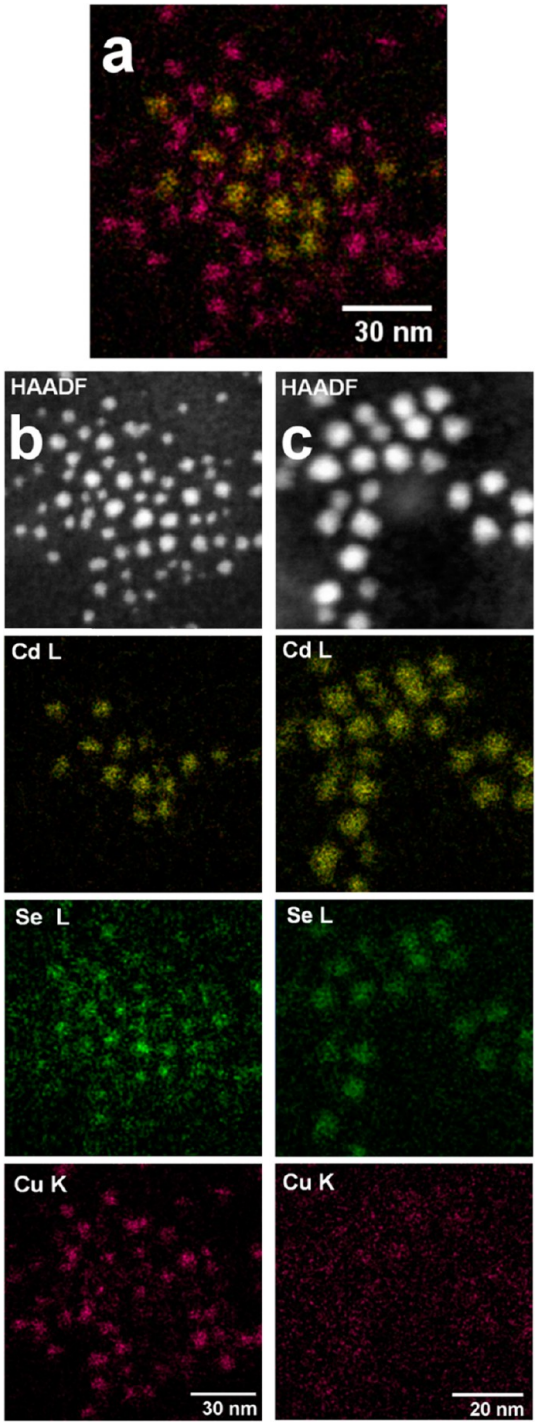

Figure 6. Scanning transmission electron microscopy (STEM) measurements of the copper incubated (2000 equiv pp) encapsulated QD: (a) Overlay of the cadmium L (yellow) and copper K (magenta) signals of PI-*b*-$(PEO)_2$ encapsulated particles; (b and c) high angular dark-field (HAADF) STEM images of the encapsulated PI-*b*-$(PEO)_2$ Y (b) and PI-*b*-PEO 5 (c). Elemental mappings of cadmium L-line (yellow), selenium L-line (green), and copper K-line (magenta).

The latter does not mean, that those particles do not contain any copper. Since the fluorescence of this sample is completely quenched, some copper must also be present in these particles, which is, however, covered by noise in the element maps. Most probably

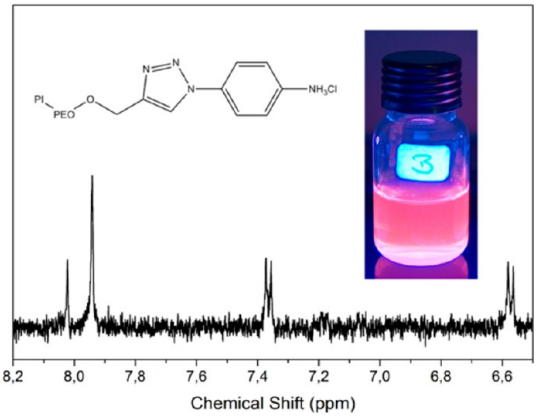

Figure 7. Aromatic region of the ^{1}H NMR spectrum of aniline hydrochloride coupled QDs, showing the signals of the aniline (6.6 and 7.4 ppm) and the signal for the aromatic triazole proton (8.1 ppm), measured in THF-d8.

the sample consisted of differently shielded QDs, some of which were easily converted into the respective copper−chalcogenide, whereas others were more resistant to ion exchange. This would be in perfect accordance to the fluorescence quenching experiments (see Figure 3).

The images for PI-*b*-PEO 5 encapsulated QDs, which showed up an extremly high resistivity against Cu^{2+} fluorescence quenching, do not differ from pure QD samples without copper addition. Consequently, no copper was found in the elemental maps (Figure 6c) again confirming the conclusions from the fluorescence data. More element maps of other samples can be found in the Supporting Information (Figures SI 11−13).

Click Chemistry. The high stability of particles encapsulated in the big polymers against copper ions led us to the investigation of copper catalyzed azide alkyne cycloaddition reactions. Therefore, a small batch of QDs was encapsulated in a blend of alkyne (∼33%) and hydroxyl functionalized (∼67%) PI-*b*-PEO, following the standard procedure of encapsulation. In four quick experiments, the coupling of 4-azido-aniline hydrochloride to the alkyne functionalized micelles was tested, varying some parameters according to literature reports.[50] We found a quick and versatile method to perform the cyclo-addition, yielding the desired product with a conversion of 20% (determined from the NMR signals for the aniline (6.6 and 7.4 ppm) and the triazole proton (8.1 ppm)). Fortunately and as expected, the particles retained their fluorescence with almost no loss (see Figure 7). For the complete NMR spectrum and further information, see Figure SI 14.

CONCLUSION

Differently sized and shaped PI-*b*-PEO diblock copolymer ligands may control the interaction of the quantum dot polymer construct leading to different properties in cellular uptake and different accessibility of the quantum dot itself. Thus, the polymer shell may avoid the contact of quenching ions and quantum dots. Herein, we presented a copper catalyzed click reaction of quantum dots maintaining their fluorescence properties, which has not been reported for the functionalization of single encapsulated QDs until now. A correlation between the density of the polymeric shell of the QDs and their accessibility by quenchers was proven with Cu and Fe ions. Further, a cellular uptake study showed a size dependent uptake behavior on two different cell lines. As a general trend, it can be stated that those coatings, which were most stable against quenchers, also showed the best resistivity with respect to unspecific cellular uptake.

EXPERIMENTAL SECTION

Chemicals. Air or water sensitive chemical compounds were handled under inert conditions (Ar) using standard Schlenk technique. Chloroform (anhydrous, amylene stabilized), dichlormethane (anhydrous, amylene stabilized), 1,1′-carbonyldiimidazole (CDI), disodium 4,7-diphenyl-1,10-phenanthroline-disulfonate, 4-azido-aniline hydrochloride, sodium ascorbate, copper(II) sulfate, 1-bromo-2,3-epoxypropane (98%), *n*-BuLi (1.6 M in *n*-hexane), 2,2′-azobis(2-methylpropionitrile) (AIBN), *s*-BuLi (1.4 M in cyclohexane), trioctylphosphine (TOP), selenium and zinc acetate were purchased from Aldrich; trioctylphosphine oxide (TOPO) and hexadecylamine (HDA) were from Merck; acetone, hydrochloric acid (37%), and tetrahydrofuran (THF) were from Grüssing; chloroform-d_1 ($CDCl_3$, 99.8%) and tetrahydrofuran-d_8 (THF-d_8, 99.9%) were from Deutero; copper(II) acetate and tetradecylphosphonic acid were from Alfa Aesar, and cadmium acetate was from ChemPur.

The synthesis of different sized PI and PI-*b*-PEO was performed according to the known procedure.[28] The conversion of 1-bromo-2,3-epoxypropane to 3-bromo-1,2-propanediol was done analogous to the described synthesis elsewhere.[51] 4-(Bromomethyl)-2,2-dimethyl-1,3-dioxolane was prepared as described elsewhere;[52] however to avoid benzene as a solvent, acetone was used. Exchange of ligands on nanoparticles was done analogous to the previously described procedure.[28]

Instrumentation. Proton nuclear magnetic resonance (^{1}H NMR) spectra were recorded on a Bruker AV I 400, AV II 400 or DRX 500 spectrometer. Chemical shifts in are reported in δ units (ppm) relative to the deuterated solvent signal ($CDCl_3$ signal at 7.26 ppm) or tetramethylsilane as an internal standard (TMS signal at 0 ppm).

Size exclusion measurements (SEC) were performed at 35 °C on a Tosoh EcoSEC HLC-8320 GPC system, using three SDV columns (Polymer Standards Service) with a porosity range of 50−1000 Å and a SDV precolumn with THF as solvent and eluent. The sample concentration was 1 mg mL^{-1}, the flow rate was set to 1 mL min^{-1}, and detection was executed with a Tosoh RI detector. PEG standards (PSS) were used for calibration.

TEM measurements were carried out with a Jeol JEM-1011 microscope (100 keV) and with a double corrected (cescor, cetcor) JEM 2200 FS. EDX Mappings were made using JED-2300 with Si(Li) detector.

Absorption measurments were made with a Cary 50 from Varian and steady-state fluorescence was measured using a Fluoromax 4 from Horiba Jobin Yvon. The fluorescence decay spectra (TRSPC) were collected with an excitation wavelength λ = 438 nm from a PDL 800-D pulsed diode laser and detected

with a PMA-M185 photomultipier with a resolution of 500 ps (PicoQuant). The signal was processed by a constant fraction 200 MHz discriminator and a time-to-amplitude converter (EG&G Ortec). Fluorescence decay curves were fitted with a stretched monoexponential using *Mathematica* and the average lifetime were calculated using the gamma function.[48] Beta for the native particles is ~0.7 and is reduced slightly within quencher addition. In the strongest quenched sample (1000 equiv) beta is about 0.5.

Synthesis of PI-*b*-(PEO)$_2$ Y (4). The polymerization of isoprene was performed, following the already mentioned procedure.[28] Instead of ethylene oxide, a slight excess of 4-(bromomethyl)-2,2-dimethyl-1,3-dioxolane (**1**) was used as terminating reagent. After evaporation of the solvent, the polymer was precipitated in methanol and dried *in vacuo*.

A total of 14.5 g (6.30 mmol) of the dioxolane-terminated PI (**2**) was dissolved in 200 mL of THF. Then, 50 mL of hydrochloric acid (4 M) was added, and the mixture was refluxed for 4 h. The mixture was stirred for another 12 h at ambient temperature, before the solvent was evaporated. The biphasic mixture was diluted with 300 mL of dichloromethane. The aqueous phase was discarded; the organic phase was washed with water (1×), saturated $NaHCO_3$ (2×), and water again before it was dried over Na_2SO_4. After evaporation of the solvent, the polymer was precipitated in methanol.

A total of 12.8 g (5.57 mmol) of the deprotected PI (**3**) was used as macroinitiator for the polymerization of ethylene oxide. The polymer was dissolved in 350 mL of dry THF. Under an argon atmosphere, 11.2 mL of diphenylmethylpotassium (~1 mmol/L in THF) was added. Then, 35 mL of ethylene oxide was dried and purified over CaH_2, sodium mirror, and *n*-BuLi before it was distilled to the activated PI solution. The polymerization was carried out for 96 h at 40 °C and finally terminated using 2 mL of acetic acid (35 mmol). After evaporation of the solvent, the polymer was precipitated in diethyl ether and cold acetone.

Synthesis of Quantum Dots. CdSe/CdS/ZnS core−shell−shell nanocrystals (CANdots Serie A, slightly modified) were prepared by CAN GmbH (Center for Applied Nanotechnology, Hamburg, Germany) based on the synthesis of Talapin *et al.*[53] Trioctylphosphine oxide (TOPO, 64 g) was dried *in vacuo* for 1 h before hexadecylamine (HDA, 40 g) and tetradecylphosphonic acid (TDPA, 1.6 g) were added, and the obtained solution was further dried *in vacuo* (120 °C, 30 min). Se-TOP (16 mL, 1 M solution) was added, and the reaction mixture was heated to 300 °C. Cadmium acetate, dissolved in TOP (24 mL, 0.17 M solution) was added *via* hot injection. The reaction mixture was stirred for 100 min at 260 °C. The solution was cooled to 90 °C, and toluene was added. The CdSe *core* Particles were precipitated using methanol and dissolved in *n*-hexane. The shell was synthesized using a solution of TOPO, HDA and TDPA, as explained above. The CdSe *core* solution was added, and the *n*-hexane was removed *in vacuo*. Cadmium acetate, dissolved in TOP (24 mL, 0.17 M), was added, and the solution was heated to 220 °C. Aliquots of hydrogen sulfide (96 mL) were added over a period of 40 min. Afterward, zinc acetate TOP solution (24 mL, 0.2 M) and hydrogen sulfide (192 mL) were added and the solution was stirred overnight. Zinc acetate TOP solution was added (12 mL, 0.2 M) and excess hydrogen sulfide was removed using nitrogen stream. The solution was cooled down and toluene was added. The *core−shell−shell* particles were precipitated with methanol three times before dissolving them in hexane.

Encapsulation of QDs in PI-*b*-PEO Block Copolymers. PI-coated quantum dots, a 300-fold excess of PI-*b*-PEO and AIBN (1/3 of isoprene units present in the diblock copolymer) were dissolved in THF to yield a 10 μM solution. This solution was injected into the 10-fold volume of water and stirred for 30 min to equilibrate. After equilibration, the solution was heated to 80 °C for 4 h to initiate cross-linking and remove excess THF. The samples were purified by ultracentrifugation using a sucrose gradient from 0% up to 60%. Excess sucrose was removed by several washing steps, using centrifugal filter units.

Quenching Experiments. The CSS QD (100 nM) were diluted in a quarz cuvette and equilibrated 15 min. Absorption, steady-state fluorescence and fluorescence decay spectra (TRSPC) were collected. Aliquots of the copper acetate solution (1.452 mM) were added and kept for 30 min in the dark before absorption, steady-state and fluorescence decay spectra were collected.

Click Reaction. The click reactions were performed based on the work of Hassane *et al.* using copper sulfate, sodium ascorbate, 4-azido-aniline hydrochloride and bathophenanthroline disulfonate.[50] The concentrations were the following: QD 1 μM, 4-azido-aniline hydrochloride 200 μM, copper sulfate 100 μM, disodium 4,7-diphenyl-1,10-phenanthrolinedisulfonat 200 μM, sodium ascorbate 500 μM. The solutions were mixed and stirred for 20 h at room temperature. The concentration of the alkine was 100 μM using a 1/3 blend of alkine functionalized PI-*b*-PEO and PI-*b*-PEO 5. Afterward, the solution was washed three times using a membrane filter and dialyzed against water. Water was removed using a freeze-dryer and the product was dissolved in in THF-d_8.

Cellular Uptake. A549 cells (10 000 cells per well) were grown in Lab-Tek thin bottom chambers to confluence, before being exposed to 1 μM nanoparticles in serum free medium. After 20 h incubation at a temperature of 37 °C in a humidified atmosphere containing 5% CO_2, cells were washed with PBS, counterstained with Hoechst 33342, and monitored by confocal laser scanning microscopy (Olympus FluoView FV1000 with an IX81 inverted microscope; CLSM).

RAW-264.7 cells (10 000 cells per well) were grown in Lab-Tek thin bottom chambers for 2 days, before being exposed to 1 μM nanoparticles in serum free medium. After 20 h incubation at a temperature of 37 °C in a humidified atmosphere containing 5% CO_2, cells were washed with PBS, counterstained with Hoechst 33342 and monitored by CLSM.

Conflict of Interest: The authors declare no competing financial interest.

Acknowledgment. This work was supported by the EU within the FP 7 program (Vibrant, EU 228933), the State Excellence Initiative "Nanotechnology in Medicine" and the Chemical Industry Fund, VCI: German Chemical Industry Association. We kindly thank CAN GmbH for the preparation and provision of the slightly modified CANdots Serie A free of charge. Further, we thank D. Meyer for the illustration of the TOC graphic.

Supporting Information Available: DLS data and TEM images of PI-*b*-PEO encapsulated QDs, additional CLSM images of A549 cells incubated with encapsulated QDs, extended information on fluorescence quenching experiments (quenching with $FeCl_3$, investigation of quenching with wide-field fluorescence imaging), additional STEM EDX mappings, NMR spectrum of aniline hydrochloride coupled QDs. This material is available free of charge *via* the Internet at http://pubs.acs.org.

REFERENCES AND NOTES

1. Medintz, I. L.; Uyeda, H. T.; Goldman, E. R.; Mattoussi, H. Quantum Dot Bioconjugates for Imaging, Labelling and Sensing. *Nat. Mater.* **2005**, *4*, 435–446.
2. Chen, O.; Zhao, J.; Chauhan, V. P.; Cui, J.; Wong, C.; Harris, D. K.; Wei, H.; Han, H.-S.; Fukumura, D.; Jain, R. K.; *et al.* Compact High-Quality CdSe-CdS Core-Shell Nanocrystals with Narrow Emission Linewidths and Suppressed Blinking. *Nat. Mater.* **2013**, *12*, 1–7.
3. Resch-Genger, U.; Grabolle, M.; Cavaliere-Jaricot, S.; Nitschke, R.; Nann, T. Quantum Dots *versus* Organic Dyes as Fluorescent Labels. *Nat. Methods* **2008**, *5*, 763–775.
4. Mekis, I.; Talapin, D. V.; Kornowski, A.; Haase, M.; Weller, H. One-Pot Synthesis of Highly Luminescent CdSe/CdS Core−Shell Nanocrystals *via* Organometallic and "Greener" Chemical Approaches. *J. Phys. Chem. B* **2003**, *107*, 7454–7462.
5. Thiry, M.; Boldt, K.; Nikolic, M. S.; Schulz, F.; Ijeh, M.; Panicker, A.; Vossmeyer, T.; Weller, H. Fluorescence Properties of Hydrophilic Semiconductor Nanoparticles with Tridentate Polyethylene Oxide Ligands. *ACS Nano* **2011**, *5*, 4965–4973.
6. Uyeda, H. T.; Medintz, I. L.; Jaiswal, J. K.; Simon, S. M.; Mattoussi, H. Synthesis of Compact Multidentate Ligands to Prepare Stable Hydrophilic Quantum Dot Fluorophores. *J. Am. Chem. Soc.* **2005**, *127*, 3870–3878.

7. Pellegrino, T.; Manna, L.; Kudera, S.; Liedl, T.; Koktysh, D.; Rogach, A. L.; Keller, S.; Ra, J.; Natile, G.; Parak, W. J. Hydrophobic Nanocrystals Coated with an Amphiphilic Polymer Shell: A General Route to Water Soluble Nanocrystals. *Nano Lett.* **2004**, *4*, 703–707.
8. Pöselt, E.; Fischer, S.; Foerster, S.; Weller, H. Highly Stable Biocompatible Inorganic Nanoparticles by Self-Assembly of Triblock-Copolymer Ligands. *Langmuir* **2009**, *25*, 13906–13913.
9. Chan, Y.; Zimmer, J. P.; Stroh, M.; Steckel, J. S.; Jain, R. K.; Bawendi, M. G. Incorporation of Luminescent Nanocrystals into Monodisperse Core-Shell Silica Microspheres. *Adv. Mater.* **2004**, *16*, 2092–2097.
10. Kloust, H.; Pöselt, E.; Kappen, S.; Schmidtke, C.; Kornowski, A.; Pauer, W.; Moritz, H.-U.; Weller, H. Ultrasmall Biocompatible Nanocomposites: a New Approach Using Seeded Emulsion Polymerization for the Encapsulation of Nanocrystals. *Langmuir* **2012**, *28*, 7276–7281.
11. Rostovtsev, V. V; Green, L. G.; Fokin, V. V; Sharpless, K. B. A Stepwise Huisgen Cycloaddition Process: Copper(I)-Catalyzed Regioselective "Ligation" of Azides and Terminal Alkynes. *Angew. Chem., Int. Ed.* **2002**, *41*, 2596–2599.
12. Brennan, J. L.; Hatzakis, N. S.; Tshikhudo, T. R.; Dirvianskyte, N.; Razumas, V.; Patkar, S.; Vind, J.; Svendsen, A.; Nolte, R. J. M.; Rowan, A. E.; *et al.* Bionanoconjugation *via* Click Chemistry: The Creation of Functional Hybrids of Lipases and Gold Nanoparticles. *Bioconjugate Chem.* **2006**, *17*, 1373–1375.
13. Boisselier, E.; Salmon, L.; Ruiz, J.; Astruc, D. How to Very Efficiently Functionalize Gold Nanoparticles by "Click" Chemistry. *Chem. Commun.* **2008**, 5788–5790.
14. Binder, W. H.; Sachsenhofer, R.; Straif, C. J.; Zirbs, R. Surface-Modified Nanoparticles *via* Thermal and Cu(I)-Mediated "Click" Chemistry: Generation of Luminescent CdSe Nanoparticles with Polar Ligands Guiding Supramolecular Recognition. *J. Mater. Chem.* **2007**, *17*, 2125–2132.
15. Beaune, G.; Tamang, S.; Bernardin, A.; Bayle-Guillemaud, P.; Fenel, D.; Schoehn, G.; Vinet, F.; Reiss, P.; Texier, I. Luminescence of Polyethylene Glycol Coated CdSeTe/ZnS and InP/ZnS Nanoparticles in the Presence of Copper Cations. *ChemPhysChem* **2011**, *12*, 2247–2254.
16. Isarov, A. V.; Chrysochoos, J. Optical and Photochemical Properties of Nonstoichiometric Cadmium Sulfide Nanoparticles: Surface Modification with Copper(II) Ions. *Langmuir* **1997**, *13*, 3142–3149.
17. Jawaid, A. M.; Chattopadhyay, S.; Wink, D. J.; Page, L. E.; Snee, P. T. Cluster-Seeded Synthesis of Doped CdSe:Cu_4 Quantum Dots. *ACS Nano* **2013**, *7*, 3190–3197.
18. Chen, D.; Viswanatha, R.; Ong, G. L.; Xie, R.; Balasubramaninan, M.; Peng, X. Temperature Dependence of "Elementary Processes" in Doping Semiconductor Nanocrystals. *J. Am. Chem. Soc.* **2009**, *131*, 9333–9339.
19. Srivastava, B. B.; Jana, S.; Pradhan, N. Doping Cu in Semiconductor Nanocrystals: Some Old and Some New Physical Insights. *J. Am. Chem. Soc.* **2011**, *133*, 1007–1015.
20. Bernardin, A.; Cazet, A.; Guyon, L.; Delannoy, P.; Vinet, F.; Bonnaffé, D.; Texier, I. Copper-Free Click Chemistry for Highly Luminescent Quantum Dot Conjugates: Application to *in Vivo* Metabolic Imaging. *Bioconjugate Chem.* **2010**, *21*, 583–588.
21. Schieber, C.; Bestetti, A.; Lim, J. P.; Ryan, A. D.; Nguyen, T.-L.; Eldridge, R.; White, A. R.; Gleeson, P. a; Donnelly, P. S.; Williams, S. J.; *et al.* Conjugation of Transferrin to Azide-Modified CdSe/ZnS Core-Shell Quantum Dots Using Cyclooctyne Click Chemistry. *Angew. Chem., Int. Ed.* **2012**, *51*, 10523–10527.
22. Zhang, P.; Liu, S.; Gao, D.; Hu, D.; Gong, P.; Sheng, Z.; Deng, J.; Ma, Y.; Cai, L. Click-Functionalized Compact Quantum Dots Protected by Multidentate-Imidazole Ligands: Conjugation-Ready Nanotags for Living-Virus Labeling and Imaging. *J. Am. Chem. Soc.* **2012**, *134*, 8388–8391.
23. Breus, V. V.; Heyes, C. D.; Nienhaus, G. U. Quenching of CdSe-ZnS Core-Shell Quantum Dot Luminescence by Water-Soluble Thiolated Ligands. *J. Phys. Chem. C* **2007**, *111*, 18589–18594.
24. Peng, P.; Sadtler, B.; Alivisatos, A. P.; Saykally, R. J. Exciton Dynamics in CdS−Ag_2S Nanorods with Tunable Composition Probed by Ultrafast Transient Absorption Spectroscopy. *J. Phys. Chem. B* **2010**, *114*, 5879–5885.
25. Boldt, K.; Jander, S.; Hoppe, K.; Weller, H. Characterization of the Organic Ligand Shell of Semiconductor Quantum Dots by Fluorescence Quenching Experiments. *ACS Nano* **2011**, *5*, 8115–8123.
26. Ji, X.; Palui, G.; Avellini, T.; Na, H. B.; Yi, C.; Knappenberger, K. L.; Mattoussi, H. On the pH-Dependent Quenching of Quantum Dot Photoluminescence by Redox Active Dopamine. *J. Am. Chem. Soc.* **2012**, *134*, 6006–6017.
27. Pons, T.; Medintz, I. L.; Sapsford, K. E.; Higashiya, S.; Grimes, A. F.; English, D. S.; Mattoussi, H. On the Quenching of Semiconductor Quantum Dot Photoluminescence by Proximal Gold Nanoparticles. *Nano Lett.* **2007**, *7*, 3157–3164.
28. Pöselt, E.; Schmidtke, C.; Fischer, S.; Peldschus, K.; Salamon, J.; Kloust, H.; Tran, H.; Pietsch, A.; Heine, M.; Adam, G.; *et al.* Tailor-Made Quantum Dot and Iron Oxide Based Contrast Agents for *in Vitro* and *in Vivo* Tumor Imaging. *ACS Nano* **2012**, *6*, 3346–3355.
29. Schmidtke, C.; Pöselt, E.; Ostermann, J.; Pietsch, A.; Kloust, H.; Tran, H.; Schotten, T.; Bastús, N. G.; Eggers, R.; Weller, H. Amphiphilic, Cross-Linkable Diblock Copolymers for Multifunctionalized Nanoparticles as Biological Probes. *Nanoscale* **2013**, *5*, 7433–7444.
30. Förster, S.; Kramer, E. Synthesis of PB-PEO and PI-PEO Block Copolymers with Alkyllithium Initiators and the Phosphazene Base t-BuP_4. *Macromolecules* **1999**, *32*, 2783–2785.
31. Allgaier, J.; Poppe, A.; Willner, L.; Richter, D. Synthesis and Characterization of Poly[1,4-isoprene-b-(ethylene oxide)] and Poly[ethylene-co-propylene-b-(ethylene oxide)] Block Copolymers. *Macromolecules* **1997**, *30*, 1582–1586.
32. Al-Jarrah, M. M. F.; Apikian, R. L.; Ahmed, E. Polymerization Mechanisms. *Polym. Bull.* **1984**, *12*, 433–436.
33. Schmidtke, C.; Lange, H.; Tran, H.; Ostermann, J.; Kloust, H.; Bastús, N. G.; Merkl, J.-P.; Thomasen, C.; Weller, H. Radical Initiated Reactions on Biocompatible CdSe-Based Quantum Dots: Ligand Crosslinking, Crystal Annealing and Fluorescence Enhancement. *J. Phys. Chem. C* **2013**, *117*, 8570–8578.
34. Zalipsky, S. Functionalized Poly(ethylene glycol) for Preparation of Biologically Relevant Conjugates. *Bioconjugate Chem.* **1995**, *6*, 150–165.
35. Natalello, A.; Tonhauser, C.; Berger-Nicoletti, E.; Frey, H. A Combined DPE/Epoxide Termination Strategy for Hydroxyl End-Functional Poly(2-vinylpyridine) and Amphiphilic AB_2-Miktoarm Stars. *Macromolecules* **2011**, *44*, 9887–9890.
36. Pispas, S.; Hadjichristidis, N.; Potemkin, I.; Khokhlov, A. Effect of Architecture on the Micellization Properties of Block Copolymers: A_2B Miktoarm Stars *vs* AB Diblocks. *Macromolecules* **2000**, *33*, 1741–1746.
37. Cai, Y.; Tang, Y.; Armes, S. P. Direct Synthesis and Stimulus-Responsive Micellization of Y-Shaped Hydrophilic Block Copolymers. *Macromolecules* **2004**, *37*, 9728–9737.
38. Soliman, G. M.; Sharma, R.; Choi, A. O.; Varshney, S. K.; Winnik, F. M.; Kakkar, A. K.; Maysinger, D. Tailoring the Efficacy of Nimodipine Drug Delivery Using Nanocarriers Based on A_2B Miktoarm Star Polymers. *Biomaterials* **2010**, *31*, 8382–8392.
39. Gibanel, S.; Forcada, J.; Heroguez, V.; Schappacher, M.; Gnanou, Y. Novel Gemini-Type Reactive Dispersants Based on PS/PEO Block Copolymers: Synthesis and Application. *Macromolecules* **2001**, *34*, 4451–4458.
40. Liu, H.; Xu, J.; Jiang, J.; Yin, J.; Narain, R.; Cai, Y.; Liu, S. Syntheses and Micellar Properties of Well-Defined Amphiphilic AB_2 and A_2B Y-Shaped Miktoarm Star Copolymers of ε-Caprolactone and 2-(Dimethylamino)ethyl Methacrylate. *J. Polym. Sci., Part A: Polym. Chem.* **2007**, *45*, 1446–1462.
41. Gao, Z.; Eisenberg, A. A Model of Micellization for Block Copolymers in Solutions. *Macromolecules* **1993**, *26*, 7353–7360.

42. Wilhelm, M.; Zhao, C.; Wang, Y.; Xu, R.; Winnik, M. A.; Mura, J.-L.; Riess, G.; Croucher, M. D. Poly(styrene-ethylene Oxide) Block Copolymer Micelle Formation in Water: a Fluorescence Probe Study. *Macromolecules* **1991**, *24*, 1033–1040.
43. Kangwansupamonkon, W.; Gilbert, R. G.; Kiatkamjornwong, S. Modification of Natural Rubber by Grafting with Hydrophilic Vinyl Monomers. *Macromol. Chem. Phys.* **2005**, *206*, 2450–2460.
44. Hühn, D.; Kantner, K.; Geidel, C.; Brandholt, S.; Cock, I. De; Soenen, S. J. H.; Rivera Gil, P.; Montenegro, J.-M.; Braeckmans, K.; Müllen, K.; *et al.* Polymer-Coated Nanoparticles Interacting with Proteins and Cells: Focusing on the Sign of the Net Charge. *ACS Nano* **2013**, *7*, 3253–3263.
45. Mahmoudi, M.; Abdelmonem, A. M.; Behzadi, S.; Clement, J. H.; Dutz, S.; Ejtehadi, M. R.; Hartmann, R.; Kantner, K.; Linne, U.; Maffre, P.; *et al.* Temperature—The "Ignored" Factor at the NanoBio Interface. *ACS Nano* **2013**, 10.1021/nn305337c.
46. Lakowicz, J. *Principles of Fluorescence Spectroscopy*; 3rd ed.; Springer: New York, 2010.
47. Beaune, G.; Tamang, S.; Bernardin, A.; Bayle-Guillemaud, P.; Fenel, D.; Schoehn, G.; Vinet, F.; Reiss, P.; Texier, I. Luminescence of Polyethylene Glycol Coated CdSeTe/ZnS and InP/ZnS Nanoparticles in the Presence of Copper Cations. *ChemPhysChem* **2011**, *12*, 2247–2254.
48. Chen, Y.; Rosenzweig, Z. Luminescent CdS Quantum Dots as Selective Ion Probes. *Anal. Chem.* **2002**, *74*, 5132–5138.
49. Kriegel, I.; Jiang, C.; Rodríguez-Fernández, J.; Schaller, R. D.; Talapin, D. V; Como, E. da; Feldmann, J. Tuning the Excitonic and Plasmonic Properties of Copper Chalcogenide Nanocrystals. *J. Am. Chem. Soc.* **2012**, *134*, 1583–1590.
50. Hassane, F. S.; Frisch, B.; Schuber, F. Targeted Liposomes: Convenient Coupling of Ligands to Preformed Vesicles Using "Click Chemistry. *Bioconjugate Chem.* **2006**, *17*, 849–854.
51. Winstein, S.; Goodman, L. Neighboring Groups in Addition. II. Hydroxyl and Acetoxy Groups in Allyl Derivatives. *J. Am. Chem. Soc.* **1954**, *76*, 4368–4372.
52. Marasco, C. J.; Piantadosi, C.; Meyer, K. L.; Morris-Natschke, S.; Ishaq, K. S.; Small, G. W.; Daniel, L. W. Synthesis and Biological Activity of Novel Quaternary Ammonium Derivatives of Alkylglycerols as Potent Inhibitors of Protein Kinase C. *J. Med. Chem.* **1990**, *33*, 985–992.
53. Talapin, D. V.; Mekis, I.; Götzinger, S.; Kornowski, A.; Benson, O.; Weller, H. CdSe/CdS/ZnS and CdSe/ZnSe/ZnS Core-Shell-Shell Nanocrystals. *J. Phys. Chem. B* **2004**, *108*, 18826–18831.